4×112 Gb/s/λ MCF Transmission Using Field PDM-PAM4 and Coherent Detection for Datacenter Applications

Yuyuan Gao, Wenpeng Gao, Ming Luo, Haibo Li, Jiahao Huo, *Associate Member, IEEE*, Dongxu Lu, and Xian Zhou

***Abstract*—The inter-data center links are meeting the challenge of increasing transmission capacity continuously. Here, the tradeoff between transmission capacity and cost and power consumption especially needs to be considered. The field modulation polarization-division-multiplexed (PDM) four-level pulse amplitude modulation (PAM4) with coherent detection is a potential candidate for 400 Gb/s and beyond inter-data center transmissions, which has several advantages including low-cost, low optical signal to noise ratio (OSNR) requirement and high receiver sensitivity. In this paper, the feasibility and effectiveness of the field PDM-PAM4 coherent system are investigated over multi core fiber (MCF). In order to adapt to the field PAM signals, the signal-phase aid least-mean square (SP-LMS) and training multi-modulus algorithm (TMMA) are modified and analyzed for equalization and polarization demultiplexing. Finally, it is demonstrated that 4×112 Gb/s field PDM-PAM4 is successful transmitted over 16 km MCF and 384 km SSMF in C-band with a BER below 3.8e-3.**

***Index Terms*—MCF, data center, coherent detection, low cost.**

I. Introduction

THE applications such as the internet of things, live streaming online and cloud computing services will be deployed rapidly in the 5G era, which makes requirement of increasing transmission bandwidth of links of intra- or inter- datacenter urgent. According to Cisco's recent forecast, global data center traffic goes up by nearly 3 ZB a year and will reach 20.6 ZB by 2021 [1]. Carrier-less amplitude and phase (CAP) modulation [2]–[4], discrete multi-tone (DMT) modulation [5], [6], and PAM [7], [8] are the modulation formats, which are suitable for intensity modulation and direct detection (IM-DD). They can provide a low-cost and power-efficiency solution to meet the requirements of the data center. Among them, demonstration about 400G transceivers using 4 x 100G 4-level pulse amplitude modulation (PAM4) signals stick out all over. Not only have they low complexity of system architecture but also performance can be safeguarded. So, they are expected to be commercialized. However, optical intensity is the only dimension that can be exploited for IMDD.

Despite increment of dependent dimensions available and absence of local oscillator (LO) laser and coherent detection for novel Stokes Vector direct detection (SVDD) [9]–[11], it also faces the defect of high required OSNR or low receiver sensitivity in unamplified links because of power-hungry analog-to-digital converters (ADCs) and digital signal processing (DSP) [12].

By comparison with the direct-detection technique, the traditional coherent detection systems used in long-haul context have the advantage in sensitivity and spectral efficiency, which can also mitigate channel dispersion. The coherent will be devolved to short-reach communication in the future, which has become a consensus in the academic circles [13]. However, due to inherent sensibility to cost, there is a challenge for a trade-off between the performance and cost in short-reach communication. There are already a variety of simplified ideas, such as analogy coherent [14], self-homodyne coherent [15], [16]. The self-homodyne coherent can remove the frequency offset estimate and carrier phase recovery, but which is only be limited to the perfect matching length between LO path and signal path. Analogy coherent means exchanging the low cost at the expense of compromising on performance.

The optical coherent systems combined with intensity modulated transmitter can effectively reduce cost, which can yet be regarded as an effective simplified coherent. The 112 Gb/s transmission over 80 km standard single mode fiber (SSMF) in C-band below a BER threshold of 3.8e-3 by using PDM-PAM4 with coherent detection was demonstrated, which is modulated by electro-absorption modulated laser (EML) [17]. The benefit is that it does not need an optical amplifier, chromatic dispersion (CD) pre-compensation, and extra carrier recovery operations. Nevertheless, limited by modulation nonlinearity, requiring a high optical signal to noise ratio (OSNR) makes it essential

Manuscript received December 19, 2021; revised January 13, 2022; accepted January 14, 2022. Date of publication January 31, 2022; date of current version February 3, 2022. This work was supported in part by the National Key Research and Development Program of China under Grant 2019YFB1803905, in part by the National Natural Science Foundation of China under Grant 62171022, in part by the Beijing Natural Science Foundation under Grant 4222009, and in part by the Guangdong Basic and Applied Basic Research Foundation under Grants 2021B1515120057 and 2020A1515111047. (*Corresponding author: Xian Zhou.*)

Yuyuan Gao, Wenpeng Gao, Jiahao Huo, Dongxu Lu, and Xian Zhou are with the Beijing Engineering and Technology Research Center for Convergence Networks and Ubiquitous Services, University of Science and Technology, Beijing 100083, China (e-mail: b20200325@xs.ustb.edu.cn; s20190635@xs.ustb.edu.cn; huojiahao@ustb.edu.cn; b20170316@xs.ustb.edu.cn; zhouxian219@ustb.edu.cn).

Ming Luo and Haibo Li are with the State Key Laboratory of Optical Communication Technologies and Networks, China Information Communication Technologies Group Corporation, Wuhan 430074, Hubei, China (e-mail: mluo@wri.com.cn; hbli@wri.com.cn).

Digital Object Identifier 10.1109/JPHOT.2022.3144298

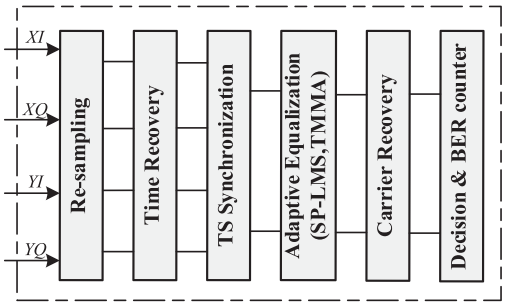

Fig. 1. Offline DSP blocks of signal recovery. TS: Training sequence.

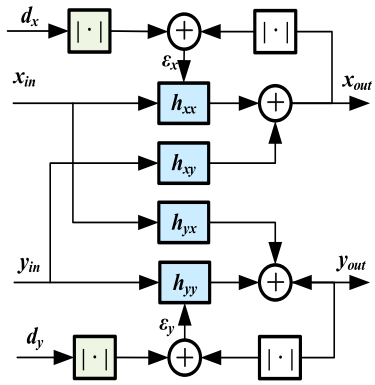

Fig. 2. Structure block of the modified TMMA algorithm.

to improve. In this paper, we improve OSNR requirement of the system by changing the intensity modulation to field PAM4 modulation which uses Mach-Zehnder modulator (MZM). Although MZM is bulky and expensive, it will use lithium niobate film material in the future, which can reduce the size and is easy to integrate. Although phase recovery is required in this system, phase recovery has a high tolerance for linewidth and low complexity due to signals carrying two-phase information. Thus, low-priced distributed feedback (DFB) lasers can be used to reduce costs. Besides, the equalization algorithm after modifying can apply to the field PAM4 signal, which has been demonstrated in this work.

Besides, the number of optical transmission channels in a unit of space is needed to increase to meet the demand of the market, which means realizing high port density. The MCF is a kind of Spatial-division multiplexing (SDM), which is an effective approach to increasing the port density, especially suitable for the short-reach data center interconnects (DCIs). Because the inter-core crosstalk is not severe and multicore amplification is not required in short reach [18]. Thus, we increase the port density by using MCF. To our best knowledge, this is the first time to transfer the field-PAM4 signal using coherent detection in MCF.

The remainder of this paper is arranged as follows. Section II gives principles of DSP at the receiver side. This will be followed by the elaborate depiction of the experimental setup, model, and parameter of equipment used in Section III. The complexity of DSP and transmission performance are discussed in Section IV. Eventually, the conclusion of the paper is presented in Section V.

II. Principle of DSP at Receiver

Fig. 1 shows the offline signal processing procedure of field PAM4 signal recovery at the receiver. The digital samples captured by the oscilloscope are resampled to two samples per symbol. The digital squaring and filter algorithm are used to solve the problem of unsynchronous between the transmitter signal clock and the ADC sampling clock. Since we transmitted signals over 400 km fiber, frequency domain equalization is used to compensate for CD. Then, in order to find the place where the training sequence (TS) begins, the cross-correlation of the received signals and the training symbols is investigated, the abscissa corresponding to the maximum value is the start point. The next step is butterfly-structured adaptive equalization that not only demultiplexes polarization but also compensates inter-symbol interferences (ISI) caused by residual CD, polarization mode dispersion (PMD), and limited bandwidth of component. Here, the equalizer tap coefficient and error function can be obtained according to the rule of modified algorithms. The detail will be described later in part A of Section II.

It is noteworthy that frequency offset estimation (FOE) and low- complexity carrier phase recovery (CPR) are necessary for this work. This is because MZM is operated at the null point for field PAM4 modulation. After the decision for symbol and mapping from symbol to bit, the BER is calculated.

A. Modified Equalization Algorithm for Felid PAM4

1) Training Multi-Modulus Algorithm (TMMA): The TMMA algorithm is a modified constant modulus algorithm (CMA) algorithm, which uses the amplitude of the signal for error calculation even in field PAM4. Therefore, the phase noise and frequency offset will not impact the robustness. The graphical representation of the equalizer function for TMMA is shown in Fig. 2.

The error functions of the n^{th} iteration are represented as follows

$$\varepsilon_x^{(n)} = \left|d_x^{(n)}\right| - \left|x_{out}^{(n)}\right|,\ \varepsilon_y^{(n)} = \left|d_y^{(n)}\right| - \left|y_{out}^{(n)}\right| \tag{1}$$

where $|\cdot|$ denotes the operation of taking modulus, and $d_{x(y)}$ stands for the reference signal of x or y polarization, which can be obtained from the training sequence. Just as basic CMA, the renewal equation of tap coefficients of filter for TMMA can be formulated as:

$$\begin{aligned}
h_{xx}^{(n+1)} &= h_{xx}^{(n)} + \mu \cdot \varepsilon_x^{(n)} \cdot x_{out}^{(n)} \cdot x_{in}^{*(n)},\\
h_{xy}^{(n+1)} &= h_{xy}^{(n)} + \mu \cdot \varepsilon_x^{(n)} \cdot x_{out}^{(n)} \cdot y_{in}^{*(n)}\\
h_{yx}^{(n+1)} &= h_{yx}^{(n)} + \mu \cdot \varepsilon_y^{(n)} \cdot y_{out}^{(n)} \cdot x_{in}^{*(n)},\\
h_{yy}^{(n+1)} &= h_{yy}^{(n)} + \mu \cdot \varepsilon_y^{(n)} \cdot y_{out}^{(n)} \cdot y_{in}^{*(n)}
\end{aligned} \tag{2}$$

where h_{xx}, h_{xy}, h_{yx} and h_{yy} denote the vectors of filter tap coefficients, x_{in} and y_{in} stand for input signal vector in X polarization and Y polarization of equalizer, μ denotes the step size of gradient descent, and $()*$ stands for operation of taking conjugate of the complex.

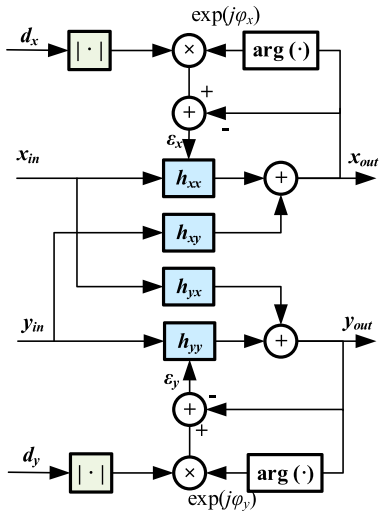

Fig. 3. Structure block of the modified SP-LMS algorithm.

Here, the training sequence is indispensable in the convergence of TMMA, but the signal cannot always be a training sequence. Therefore, the equalizer will be switched to *Decision-Directed* (*DD*) *Mode* after arriving at the convergence state. At this stage, $d_{x(y)}$ is substituted by judgment value of the output of equalizer, which can be formulated as

$$d_x^{(n)} = Decision\left(\left|x_{out}^{(n)}\right|\right),\ d_y^{(n)} = Decision\left(\left|y_{out}^{(n)}\right|\right) \quad (3)$$

2) Signal-Phase Aided Least-Mean-Square Algorithm (SP-LMS): Although we used field PAM4 signal, the phase-induced influence can be avoided by using the modulus of the reference signal, which does not influence the performance due to wide phase interval. The architecture of the SP-LMS algorithm is illustrated in Fig. 3.

The error function can be obtained by making difference between equalized signal and rotated modulus of reference signal, which n_{th} iteration are represented as follows

$$\begin{aligned} \varepsilon_x^{(n)} &= \left|d_x^{(n)}\right| \cdot \exp\left(j\varphi_x^{(n)}\right) - x_{out}^{(n)}, \\ \varepsilon_y^{(n)} &= \left|d_y^{(n)}\right| \cdot \exp\left(j\varphi_y^{(n)}\right) - y_{out}^{(n)} \end{aligned} \quad (4)$$

where $d_{x(y)}$ stands for the field PAM4 reference signal, $\varphi_{x(y)}$ denotes angles modulus of reference signal needs to rotate, which can be simply obtained by

$$\varphi_x^{(n)} = \arg\left(x_{out}^{(n)}\right),\ \varphi_y^{(n)} = \arg\left(y_{out}^{(n)}\right) \quad (5)$$

According to the stochastic gradient algorithm, the renewal equation of coefficients of butterfly filter tap for SP-LMS is formulated as,

$$\begin{aligned} h_{xx}^{(n+1)} &= h_{xx}^{(n)} + \mu \cdot \varepsilon_x^{(n)} \cdot x_{in}^{*(n)}, \\ h_{xy}^{(n+1)} &= h_{xy}^{(n)} + \mu \cdot \varepsilon_x^{(n)} \cdot y_{in}^{*(n)} \\ h_{yx}^{(n+1)} &= h_{yx}^{(n)} + \mu \cdot \varepsilon_y^{(n)} \cdot x_{in}^{*(n)}, \\ h_{yy}^{(n+1)} &= h_{yy}^{(n)} + \mu \cdot \varepsilon_y^{(n)} \cdot y_{in}^{*(n)} \end{aligned} \quad (6)$$

When the equalizer is converged, conversion from training mode to DD mode needs to be implemented. Again, the process was very similar to TMMA introduced in the previous part.

B. Phase Recovery and Frequency Offset Estimation

After adaptive equalization based on modified SP-LMS or TMMA, the k_{th} output signal from equalizer can be expressed as

$$S_k = A_k \cdot \exp\left(j\left(2\pi\Delta f\, kT_s + \theta_k + \varphi_n^k\right)\right) + n\left(k\right) \quad (7)$$

where Δf denotes the frequency offset between the transmitter laser and LO laser, A_k and θ_k denote amplitude and phase of modulating signal. T_s is the symbol interval, φ_n^k marks the k_{th} random phase noise of laser and $n(k)$ denotes the ASE noise.

Since we use field PAM-4, we need to recover the frequency and phase of the carrier. Here, we select an uncomplicated FOE algorithm based on FFT to remove effects of frequency offset on syst, and the predicted frequency offset is formulated as

$$\begin{aligned} \widetilde{\Delta f} = &\ find \\ &\left(\left|FFT\left(\left(S_k\right)^4\right)\right| == \max\left|FFT\left(\left(S_k\right)^4\right)\right|\right)/N/T_s \end{aligned} \quad (8)$$

where N is the length of the input signal, *FFT* $(\cdot)$ is Fourier transform operation.

Thus, the signal removed the FOE can be expressed as

$$S_k' = S_k \cdot \exp\left(-j\left(2\pi\widetilde{\Delta f} kT_s\right)\right) \quad (9)$$

In this case, the signal with phase noise is similar to 16 QAM, which can be classified into two rings. The carrier phase recovery algorithm such as the blind phase search (BPS) is also suitable for field PAM4 after modifying the decision. The real part of the signal after decision is ignored. Here, we employed pure feedforward structure to compensate the phase noise of a laser, the input symbol-rate sample S_k' is rotated by test phase angles φ_b,

$$\varphi_b = \frac{b}{B} \cdot \frac{\pi}{2} - \frac{\pi}{4} \quad (10)$$

where *B* stands for the amount of the test phase used, and the rotated symbol can be represented as

$$z\ (k,b) = S_k' \cdot \exp\left(j\varphi_b\right) \quad (11)$$

Then the rotated symbol is loaded to the judgment circuit, and the decision circuit outputs the ideal constellation point with the closest Euclidean distance to the input signal. The squared distance between the ideal constellation point and the rotated signal containing phase can be expressed as

$$\left|d_{k,b}\right|^2 = \left|z\left(k,b\right) - decision\left(imag\left(z\left(k,b\right)\right)\right)\right|^2 \quad (12)$$

In order to further filter out other additive noise that may exist in the receiver, the squared distances of consecutive 2N constellation points are summed to obtain

$$S_{k,b} = \sum_{-N}^{N} \left|d_{k-n,b}\right|^2 \quad (13)$$

where 2N is the number of symbols for averaging window length. Finally, the test phase corresponding to the minimum value of

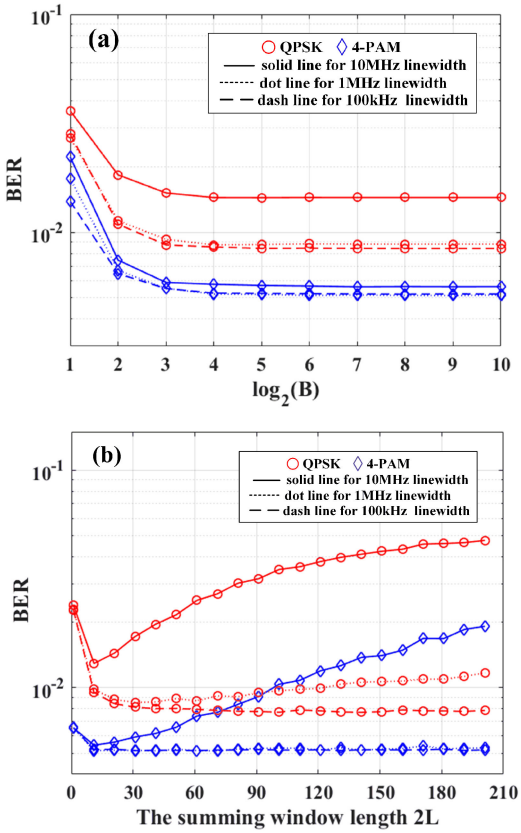

Fig. 4. The measured BER performance as function of (a) Summing window length of 2L and (b) the number of test phase of B at linewidth of 100 kHz, 1 MHz and 10 MHz for PAM4 and QPSK.

the square and distance is selected from the B test values as the estimated phase noise.

Because the PAM4 signal only carries two-phase information, which means it's possible to reduce the complexity and increase the tolerance for linewidth. Thus, we concentrate on the compensation characteristics of phase noise induced by different linewidth using different algorithm parameters. The 28-Gbaud QPSK is carried out to compare with 28-Gbaud 4PAM. Here, we neglected other impairments induced by timing clock sampling error, CD, PMD, and frequency offset to get on with the tolerance of phase noise without distractions.

To compare the performance of different modulation formats fairly, the "ASE-noise limited" OSNRs attaining a BER of 3.8e-3 are set differently for PAM4 and QPSK systems, which are corresponding to 15.67-dB and 13.63-dB respectively. Besides, differential coding/decoding technology is applied to prevent the effect of cycle slips induced by the use of CPR and get a steady BER in encoded and decision operation, but it will result in ∼0.6-dB and 0.3-dB OSNR penalty for QPSK and PAM4 respectively [19]. Fig. 4(a) depicts the BER as a function of the amount of test phase at linewidths of 100 kHz, 1 MHz, and 10 MHz with PAM4 and QPSK modulation format, respectively. It can be seen that BER performance improves primitively and hold steady along with the rise of B. However, there is no obvious penalty when $B>8$, which means that the quantization of the carrier phase noise is precise enough for both QPSK and PAM4. However, when linewidth is increased from 1 MHz to 10 MHz, the deterioration of BER performance in QPSK was more serious than 4-PAM in the same test phase angles. In Fig. 4(b), the effects of window length on BER are also inspected in identical simulation parameters. The same case also appears in Fig. 4(b). Even when linewidth is increased from 100 kHz to 1 MHz, BER performance of QPSK deterioration was worse than 4-PAM obviously, especially for large window length, which means that 4PAM have better tolerance to linewidth in the same complexity. For a 28-Gbaud 4PAM signal, the system can tolerate a corresponding laser linewidth of 10 MHz, which means that DFB lasers can replace ECLs to reduce the cost in most cases.

III. Experiment Setup

Fig. 5 shows the experiment setup. In the transmitter, a multiport tunable laser source N7714A from Agilent was used to produce a carrier that was modulated with 28 GBaud PAM4 signals, which linewidth is under 100 kHz. The center frequency was set at 1550.32 nm. The 28 GBaud PAM4 signals shaped by root-raised pulse were generated by MATLAB and then was fed into a four-channel arbitrary waveform generator (Keysight AWG M8195A). The MZM is driven by the AWG operated at 64 GS/s with a 3 dB bandwidth of 20 GHz. In order to reduce the nonlinearity distortion induced by MZM, the driving voltage of AWG was set to 120 mV. Here, MZM was operated at the null point to realize a field modulation PAM4. The polarization beam combiner combines X polarization and Y polarization signal. Then, the signal was amplified by erbium-dropped-fiber amplifiers (EDFA). Although we only have 4 km MCF, we build a loop that included 4 km MCF and 96 km SMF which was selected due to measurement of the OSNR. To alleviate the significant inter-core crosstalk of MCF, we only selected 3 outer cores and 1 middle core to transmit signals, which are marked in yellow circles in insert (ii). The remaining cores can propagate signals in opposite directions. The effectiveness of this bidirectional assignment method between neighboring cores was demonstrated in [20]. A variable optical attenuator (VOA) placed in front of EDFA was used to change the OSNR of recirculating transmission loops. Inset (i) shows the optical spectrum of the modulated signal after changing OSNR. Additionally, each loop contained an EDFA, an optical bandpass optical filter, which is used to lift the received optical power and filter the out-band noise, respectively. A timing control was used to control the loading and recirculation time of the loop gate the receiver for measurement of the transmission distance under test. The input of the loop was controlled by acousto-optic-modulators (AOM) from G & H and independent drivers. And optical switches with zero frequency. The recirculation time was controlled by another AOM switches with an 80 MHz frequency upshift. Finally, the 400 km transmission link contained 16 km MCF and 384 km SMF was realized after circulating 4 times. Optical signals passing through fiber are transmitted to an integrated coherent receiver (ICR) from Fujitsu. The optical LO is generated from another channel of a tunable laser source with 8 dBm power. Making sure polarization is aligned with the signal is necessary, which can be implemented by a polarization controller (PC). A digital oscilloscope with 60 GHz 3dB bandwidth is adopted

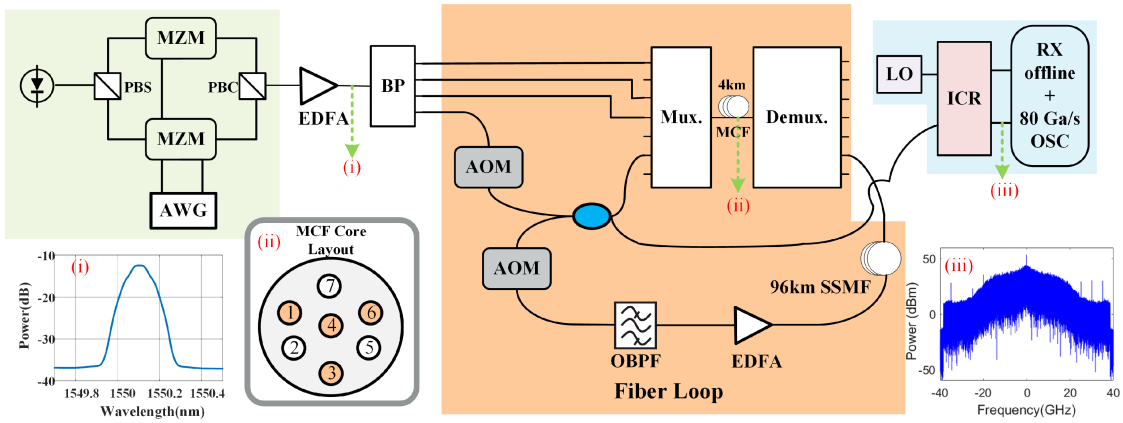

Fig. 5. Experimental setup of the 448 Gb/s field PDM-PAM4 with the coherent system. PBS: Polarization beam splitter; PBC: Polarization beam combiner; MCF: multi-core fiber; BP: 1:4 beam splitter; OBPF: Optical bandpass filter; Insets: (i) the optical spectrum of the signal after the PBC (ii) the MCF core layout (iii) the optical spectrum of the signal captured by OSC in Y-polarization.

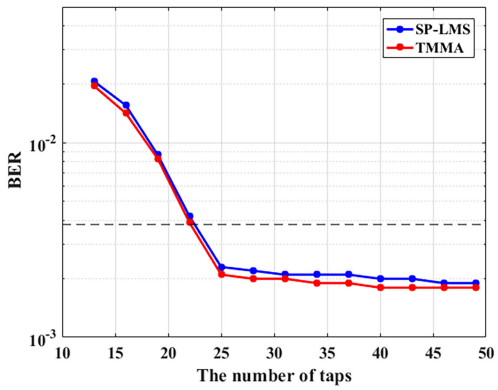

Fig. 6. BER as a function of the number of taps.

to capture the signal from ADC at a sampling rate of 80 GSa/s. Finally, the signal with all kinds of impairment was compensated by DSP offline, the DSP procedure is depicted in Fig. 1.

IV. Results and Discussion

Nyquist pulse shaping is used to remove the ISI caused by the bandwidth limitation of devices, such as DAC and MZM. Here, we used the root rise cosine (RRC) filter function of MATLAB. The BER performance is scanned under different roll-off. And 0.8 of the roll-off factor is found to realize optimal BER performance. In the first, optimal tap number of equalization is investigated. The relationship of the tap number of equalization and BER over 400 km fiber transmission at an OSNR of 22.08 dB for SP-LMS and TMMA is depicted in Fig. 6, respectively. If there is no special mention, the OSNR and transmission distance are fixed. Besides, it is worth noting that investigations about optimal parameters of equalization all use Training Mode. As shown in Fig. 6, 25 taps are enough to implement polarization demultiplex and compensate polarization mode dispersion and residual chromatic dispersion simultaneously using SP-LMS and TMMA. And TMMA is better than SP-LMS slightly can be noted.

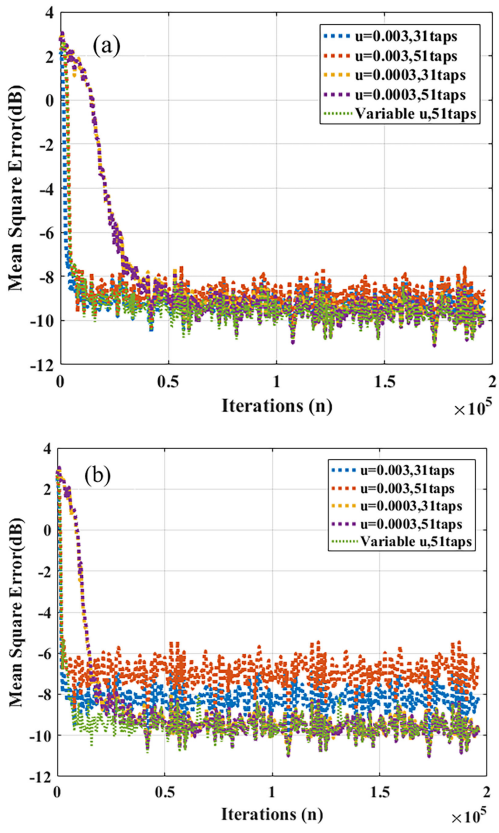

Fig. 7. MSE versus iterations with different step size parameter and different tap number using (a) SP-LMS and (b) TMMA. (After 400 km transmission, OSNR = 22.08 dB).

Secondly, after considering different parameters synthetically, speed of convergence and precision are investigated. Figure 7(a) and (b) show the mean square error as a function of iterations in the case of using SP-LMS and TMMA, respectively. It is easy to note that TMMA has a faster convergence speed than SP-LMS. Also, a larger step size has a faster convergence speed. However, it will pay dearly for larger residual error, especially for TMMA.

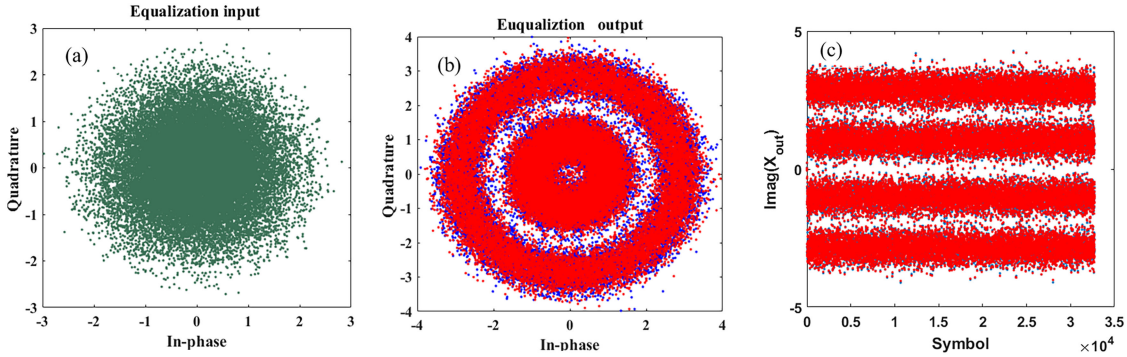

Fig. 8. Constellations of X-pol (a) Before equalization, (b) After equalization, and (c) the imagine part of the output of carrier recovery.

In the terms of tap number, results are divided into two cases. It is difficult to inspect dissimilarity on the magnitude of convergent MSE for SP-LMS. But things are different in TMMA. When the step size equals 0.003, 31 taps are better than 51 taps. Besides, the speed of convergent is affected by step size, which inspires us to use variable step size μ. μ is set to be 0.003 at first, and it is cut down by 10% when MSE is smaller than -7 dB. As shown in Fig. 7, both SP-LMS and TMMA can attain their optimum performance with speedy convergence speed by using variable step sizes. Although compared to TMMA, the profits are limited using variable μ for SP-LMS.

The constellations of the signal before and after equalization were shown in Fig. 8(a) and (b). It can be seen that the constellation of equalization output signal was classified into two rings dividually, which demonstrates that ISI has been removed after using the modified SP-LMS and TMMA. Since the phase carries information, the carrier recovery introduced by Section II needs to be done. After frequency offset estimation and carrier phase recovery were implemented, the imagined part value of the signal can be obtained, just as Fig. 8(c) shows, which means that impairment of the transmitted symbol was compensated perfectly. The red dot coincides with the blue dot, which shows that the performance is similar between TMMA and SP-LMS.

The system is not always operated in the training state in practice. Thus, the focus is on the switch operation from *Training Mode* to *DD Mode*. In the *DD Mode* stage, known training symbols will be substituted by decision values of equalization output, which has been shown in (5). In order to find the least number of TS, BER is measured for different TS numbers. The relation of them is depicted in Fig. 9. As shown in Fig. 9, the TMMA algorithm reaches the convergence condition with a fewer number of TS than that of SP-LMS. The tap number will also influence convergence speed. However, the impact of both tap number and equalization algorithm on convergence speed can be ignored.

After optimizing parameters of DSP, the performance of BER versus OSNR for BTB and 400 km mixed fiber transmission are scanned by using the optimal parameters, respectively, just as shown in Fig. 10, which means that a 448 Gb/s transmission over 400 km SSMF and MCF below a BER threshold of 3.8e-3 was demonstrated, namely, using field PDM-PAM4 with coherent detection is feasible in performance.

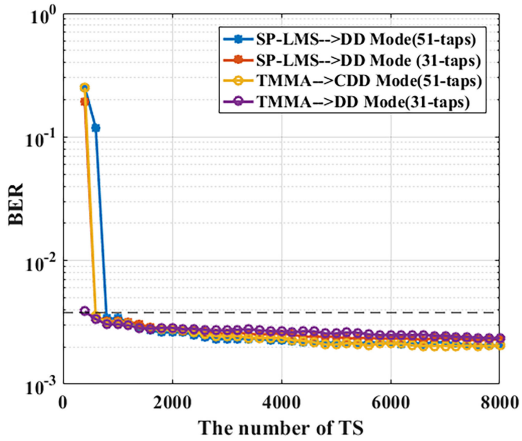

Fig. 9. BER as a function of the number of training symbols before switching.

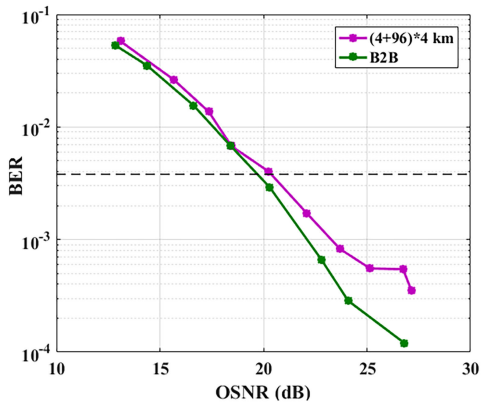

Fig. 10. BER as a function of OSNR by using TMMA algorithm.

As explained in Section III, we have no alternative but to increase the length of the loop by series connecting with 96 km SMF due to measurement of the OSNR. Despite this, a loop that included 4 km MCF and 10 km SMF was built, which was circulated 10 times, ie transmission of 40 km in MCF. For sake of verifying different cores, core 1, core 3, core 4, and core 6 was switched on loop, respectively. The BER of them was summarized in Table I, which further shows that inter-core crosstalk of MCF is not severe.

TABLE I
BER OF DIFFERENT CORES

	core 1	core 3	core 4	core 6
BER	7.93e-4	7.157e-4	7.157e-4	9.04e-4

V. CONCLUSION

In this paper, a transmission of 448 Gb/s field PDM-PAM4 over 400 km mixed fiber (SSMF and MCF) in C-band below a BER threshold of 3.8e-3 has been demonstrated by using coherent detection successfully. The SP-LMS and TMMA algorithms are modified and used to equalize the field PAM4 signal. Based on simulation and experimental analysis, the two modified algorithms have a negligible difference in OSNR requirements between BTB and transmission scenarios. Besides, it is demonstrated that the inter-core crosstalk of MCF is not severe by using un-adjacent cores in the short-reach ER application. Due to the compatibility with the large linewidth DFB laser, the PDM-PAM4 coherent system is expected to be a potential solution in the future.

REFERENCES

[1] "Cisco global cloud index: Forecast and methodology," 2016–2021 white paper, Accessed: June 6, 2018. [Online]. Available: https://www.cisco.com/c/en/us/solutions/collateral/service-provider/global-cloud-index-gci/white-paper-c11-738085.html

[2] J. Huo *et al.*, "Transmitter and receiver DSP for 112 Gbit/s PAM-4 amplifier-less transmissions using 25G-class EML and APD," *Opt. Exp.*, vol. 26, no. 18, pp. 22673–22686, Sep. 2018.

[3] S. Sao *et al.*, "Optical PAM-4 signal generation using a silicon Mach-Zehnder optical modulator," *Opt. Exp.*, vol. 25, no. 19, pp. 23003–23013, Sep. 2017.

[4] K. Zhong *et al.*, "140-Gb/s 20-km transmission of PAM-4 signal at 1.3 μm for short reach communications," *IEEE Photon. Technol. Lett.*, vol. 27, no. 16, pp. 1757–1760, Aug. 2015.

[5] F. Li *et al.*, "Experimental demonstration of four-channel WDM 560 Gbit/s 128QAM-DMT using IM/DD for 2-km optical interconnect," *J. Lightw. Technol.*, vol. 35, no. 4, pp. 941–948, Feb. 2017.

[6] T. Tanaka *et al.*, "Experimental demonstration of 448-Gbps+ DMT transmission over 30-km SMF," in *Proc. Opt. Fiber Commun.*, San Francisco, CA, USA, 2014, Paper M2I.5.

[7] J. Wei *et al.*, "100-Gb/s hybrid multiband CAP/QAM signal transmission over a single wavelength," *J. Lightw. Technol.*, vol. 33, no. 2, pp. 415–423, Jan. 2015.

[8] A. Dochhan *et al.*, "Solutions for 80 km DWDM systems," *J. Lightw. Technol.*, vol. 24, no. 2, pp. 491–499, Oct. 2016.

[9] T. Hoang *et al.*, "Enabling high-capacity long-reach direct detection transmission with QAM-PAM stokes vector modulation," *J. Lightw. Technol.*, vol. 36, no. 2, pp. 460–467, Jan. 2018.

[10] D. Che, C. Sun, and W. Shieh, "Maximizing the spectral efficiency of stokes vector receiver with optical field recovery," *Opt. Exp.*, vol. 26, no. 22, pp. 28976–28981, Oct. 2018.

[11] D. Che, C. Sun, and W. Shieh, "Optical field recovery in stokes space," *J. Lightw. Technol.*, vol. 37, no. 2, pp. 451–460, Jan. 2019.

[12] J. K. Perin, A. Shastri, and J. M. Kahn, "Data center links beyond 100 Gbit/s per wavelength," *Opt. Fiber Technol.*, vol. 44, no. 8, pp. 69–85, Aug. 2018.

[13] K. Zhong *et al.*, "Digital signal processing for short-reach optical communications: A review of current technologies and future trends," *J. Lightw. Technol.*, vol. 36, no. 2, pp. 377–400, 2018.

[14] T. Hirokawa. *et al.*, "Analog coherent detection for energy efficient intra-data center links at 200 Gbps per wavelength," *J. Lightw. Technol.*, vol. 39, no. 2, pp. 520–531, 2020.

[15] X. Zhou *et al.*, "Theoretical analysis of phase noise induced by laser linewidth and mismatch length in self-homodyne coherent systems," *J. Lightw. Technol.*, vol. 39, no. 5, pp. 1312–1321, 2020.

[16] T. Gui *et al.*, "Real-time demonstration of homodyne coherent bidirectional transmission for next-generation data center interconnects," *J. Lightw. Technol.*, vol. 39, no. 4, pp. 1231–1328, Feb. 2021.

[17] X. Zhou *et al.*, "112 Gb/s transmission over 80 km SSMF using PDM-PAM4 and coherent detection without optical amplifier," *Opt. Exp.*, vol. 24, no. 15, pp. 17359–17371, 2016.

[18] K. Saitoh and S. Matsuo, "Multicore fiber technology," *J. Lightw. Technol.*, vol. 34, no. 1, pp. 55–66, Jan. 2016.

[19] J. M. Kahn and K.-P. Ho, "Spectral efficiency limits and modulation/detection techniques for DWDM systems," *IEEE J. Sel. Topics Quantum Electron.*, vol. 10, no. 2, pp. 259–272, Mar/Apr. 2004.

[20] T. Ito *et al.*, "Reduction of influence of inter-core cross-talk in MCF with bidirectional assignment between neighboring cores," in *Proc. Opt. Fiber Commun.*, Anaheim, CA, USA, 2013, Paper OTh3K.2.